Final State Effect for Au 4f Line from Gold-nano Particles Grown on Oxides and HOPG Supports

Y. Kitsudo[1], A. Iwamoto[1], H. Matsumoto[1], K, Mitsuhara[1], T. Nishimura[1], M. Takizawa[2], T. Akita[3], Y. Maeda[3], and Y. Kido[1]

Abstract

The effect of a positive charge left to a small metal particle immediately after photoemission, so called the final state effect is studied for Au 4f binding energy (E_B) shifts. The size and shape of Au-nano-particles were determined by high-resolution medium energy ion scattering combined with scanning electron microscopy of a field emission type. The shape of Au nano-particels is well approximated by a partial sphere with diameter d and height h. It is found that the E_B shift is well expressed as number of atoms per particle (n_A) and independent of support species. The E_B shift changes dramatically at a critical n_A value of ~ 70 atoms, where metal-nonmetal transition takes place. In the nonmetal region, the E_B shift increases steeply almost exponentially with decreasing n_A and in contrast, gradually decreases with increasing n_A in the metallic region. The effect of the positive charge of an Au 4f vacancy created by photoemission is expressed by the relaxation time τ and the effective charge $+\alpha e$ when the photoelectron just leaves the Au particle surface (e: electron charge, $\alpha < 1$).

[1] *Department of Physics, Ritsumeikan University, Kusatsu, Shiga-ken 525-8577, Japan*

[2] *SR-Center, Ritsumeikan University, Kusatsu, Shiga-ken 525-8577, Japan*

[3] *Advanced Industrial Science and Technology, AIST, Ikeda, Osaka 563-8577, Japan*

I. INTRODUCTION

Au nano-particles dispersed on metal oxide supports have recently attracted much attention because of a dramatic change of catalytic activities at a critical particle size about several nm[1-6]. So far, several models have been proposed to explain the emerging catalytic activities. First principles calculations based on the density functional theory (DFT) predict importance of electronic charge transfer between Au nano-particles and supports [7-11]. For Au/MgO(001), Sanchez et al.[7] claimed that Au_8 clusters adsorbed to oxygen vacancies on the MgO surface are negatively charged and thus weaken the molecular bond of O_2. In contrast, Wang and Hammer[11] demonstrated the fact that Au_7 clusters adsorbed on an O-rich TiO_2(110) surface are cationic and consequently become highly active for oxidation of CO. For Au nano-particles on reduced TiO_2(110), the O 2p non-bonding peak shifts toward the Fermi level and the intensity of the Ti 3d surface state decreases with increasing Au coverage [10, 12]. This may be due to electron charge transfer from the surface defects to the Au particles [10]. In order to judge whether an electronic charge transfer takes place from Au to support or vice versa, Au 4f core level shifts are frequently observed and invoked. For Au on reduced and stoichiometric TiO_2(110), the Au 4f line shows higher binding energy shifts at small Au coverage [12-14]. However, the higher binding energy (E_B) shift is also induced by the effect of a photo-hole remaining on metal nano-clusters during the photoemission process, so called final state effect[12-19]. Therefore, it is crucial to characterize the final state effect in terms of size and shape of Au nano-particles and of dependence upon support species quantitatively.

In this study, we observed the core level shift of Au 4f for Au nano-particles grown on various kinds of substrates using synchrotron-radiation(SR)-light. Simultaneously, the shape and size of the Au nano-particles are determined by high resolution medium energy ion scattering (MEIS) combined with scanning electron microscopy of a field emission type (FE-SEM). Au deposition was made by molecular beam epitaxy (MBE) with Au coverage from 0.05 up to 10 ML. All the above experiments were performed *in situ* under ultra-high vacuum (UHV) conditions ($\leq 2\times10^{-10}$ Torr) except for FE-SEM observation. The present study reveals that the E_B shift of the Au 4f line is related intimately to the number of Au atoms per particle and independent of substrate species and thus it evidences that the final state effect is the primary cause of the higher E_B shifts. Finally, a new model which characterize the final state effect is proposed.

II. EXPERIMENT

The experiment was carried out at Beam-line 8 of a storage ring named AURORA working at Ritsumeikan SR Center. This beam-line combines photoelectrons spectroscopy (PES) with high-resolution MEIS and molecular beam epitaxy (MBE) systems[20]. Emitted SR photons are collected by a cylindrical mirror and monochromated with two types of varied spacing plane gratings, which cover the energy range from 10 up to 500 eV[21]. The incident photon energy was calibrated precisely using primary and the 2nd harmonic waves for Au 4 $f_{5/2,7/2}$ lines. A hemispherical electrostatic analyzer (ESA) detected emitted photoelectrons with an energy resolution of ~0.05 eV at a pass energy of 2.95 eV. The detailed specification of our toroidal ESA for MEIS analysis was described elsewhere[22] and the excellent energy resolution ($\Delta E / E = 9 \times 10^{-4}$) allowed one to determine the shape and size of Au nano-particles[23].

We prepared clean surfaces of various kinds of substrates, stoichiometric (S)- and reduced (R)-TiO_2(110), TiO_2-terminated $SrTiO_3$(001), NiO(111)/Ni(111), AlO_x /NiAl(110), and HOPG sputtered by 1 keV Ar^+ (Sp-HOPG). Annealing non-doped TiO_2(110) substrates at 700° C for 15 min in UHV led to an n-type semiconductor. After sputtering by 0.75 keV Ar^+, bridging oxygen vacancies were then induced by annealing at 550° C for 5 min in UHV. S-TiO_2(110) surfaces were obtained by exposure to O_2 at room temperature (RT) with an exposure of 1,000 L (1 L: 10^{-6} Torr s). No bridging oxygen vacancies were confirmed by observation of valence band spectra[12]. For Nd-doped $SrTiO_3$(001) and NiO(001) substrates, annealing at 500° C in O_2-ambient led to the clean (1×1) surfaces[24,25]. How to prepare clean NiO(111)/Ni(111) and AlO_x/NiAl(110) was reported previously[26,27]. Au was then deposited on the clean surfaces at RT with a Knudsen cell at a rate of 0.30 ML/min. Here, 1 ML means 1.39×10^{15} atoms/cm^2, corresponding to the areal density of Au(111). The absolute amount of the deposited Au was determined by MEIS using 120 keV He^+ ions. The analysis method how to determine the shape (two- or three-dimensional islands, sphere or cubic islands etc) and size of Au nano-particles by high-resolution MEIS is described minutely in the literature[23]. In order to confirm the validity of the present MEIS analysis, we also performed *ex situ* FE-SEM (HITACHI S-5000) observation at AIST, Kansai Center.

III. RESULT AND DISCUSSION

We observed the Au $4f_{5/2,7/2}$ spectra for Au nano-particles on various kinds of substrates at photon energy (ω Å) of 140 eV. Figure 1 shows the Au $4f_{5/2,7/2}$ spectra observed for Au/$SrTiO_3$(001) as a function of Au coverage from 0.15 up to 5.0 ML under normal emission condition. The Au $4f_{7/2}$ ($4f_{5/2}$) peak shifts to higher binding energy (E_B) side by 0.25 eV at Au coverage of 0.15 ML and gradually approaches the E_B value of bulk Au (84.0 eV) and coincides with that at Au coverage of 8 ML. The E_B shifts of Au $4f_{7/2}$ are shown in Fig. 2 for Au nano-particles grown on various kinds of supports as a function of Au coverage. It is clearly seen that the E_B shift tends to increase with decreasing Au coverage. However, relatively small E_B shifts was observed for R-TiO_2(110) and no E_B shift was seen for NiO(001) and HOPG substrates. It must be noted here that two-dimensional(2D) islands with relatively large lateral size are dominant for NiO(001) at small Au coverage[25] and large branching islands grow even at small Au coverage for HOPG[28], which will be shown later. In this paper, we define the 2D-island as that with one atomic-layer height (0.235 nm: Au(111)). As mentioned in the previous report[23], it is difficult to determine the lateral size of 2D islands. For R-TiO_2(110) support 3D-islnads start to grow from an early stage of Au

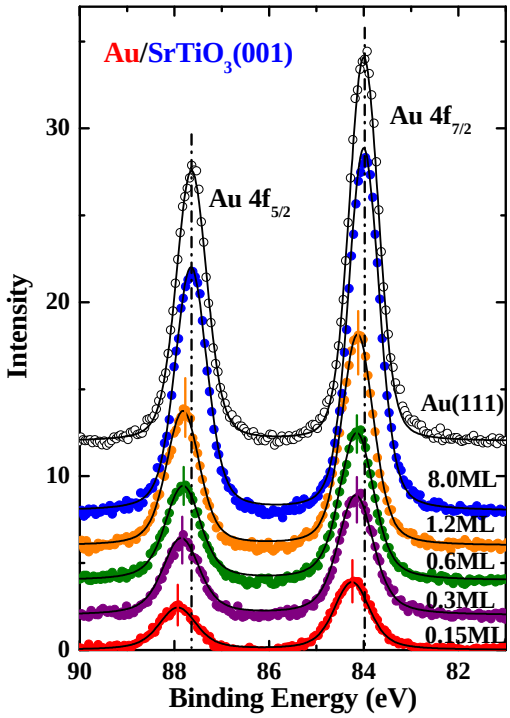

FIG. 1. Au $4f_{5/2,7/2}$ spectra observed at photon energy of 140 eV for Au/$SrTiO_3$ (001) as a function of Au coverage.

deposition owing to bridging O-vacancies acting as a nucleation site and thus larger 3D-islnads are formed compared with S-TiO_2(110) substrate at a same Au coverage[12,23]. It is emphasized that the higher E_B shifts do not come from charging of substrates due to secondary electrons emission, because all the substrates used here are conductive. This was confirmed by observing valence band and core level spectra (O 2s, Ti $3p_{1/2,3/2}$ and Sr $4p_{1/2,3/2}$) from the substrates before and after Au deposition.

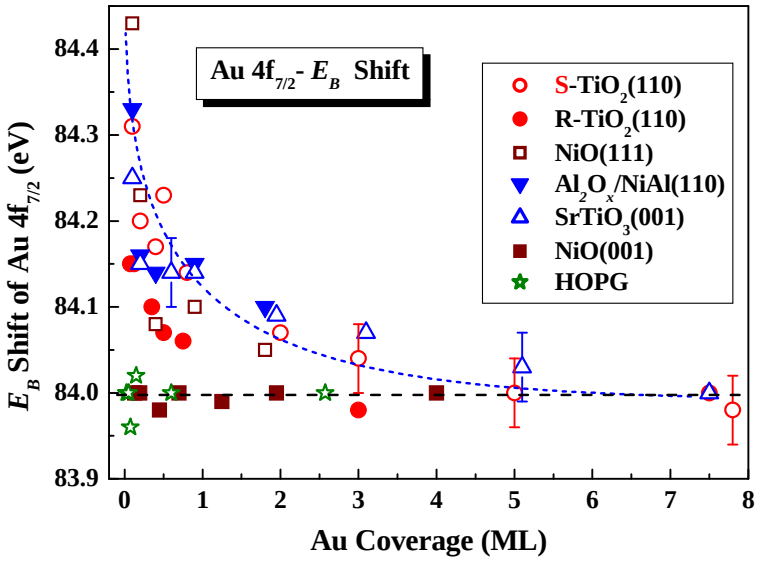

FIG. 2. Binding energy (E_B) of Au $4f_{7/2}$ line observed for various kinds of supports, as a function of Au coverage. SR-photons with energy of 140 eV were incident at an angle of 54.7° and emitted photoelectrons were detected at 0° with respect to surface normal.

As reported previously[12,25], 2D-islands grow initially and then 3D-islands are formed with increasing Au coverage for oxides supports. The shape of 3D-islands grown on oxide supports (TiO_2(110) and NiO(001)) were well approximated by a partial sphere rather than cuboid. Indeed, a circular lateral shape was observed by FE-SEM for $SrTiO_3$(001), R- and S-TiO_2(110) and NiO(001) substrates except for HOPG. High resolution MEIS allows one to distinguish the contributions from 2D- and 3D-islands and to determine the areal occupation ratios of 2D- and 3D-islands and the diameter (d) and height (h) of 3D-islands together with the fluctuations[22]. In the present MEIS analysis, the stopping power of Au and the He^+ charge fractions were determined in advance using poly-crystal Au films formed on slightly oxidized Si(111) substrates[23]. We employed the Lindhard-Scharff formula[29] for energy straggling and adopted a

symmetric Gaussian line shape. Actually, for Au nano-particles no significant difference is seen between the simulated spectra using symmetric and asymmetric line shapes. Figure 3 indicates the *d* and *h* values for S-TiO_2(110) and $SrTiO_3$(001) substrates as a function of Au coverage. At an initial stage of Au deposition the lateral size (diameter) is constant and above a critical size (2.0 nm for S-TiO_2 and 2.2 nm for $SrTiO_3$) the diameter increases almost linearly with increasing Au coverage. In the present MEIS analysis, we assumed the atomic number density of bulk Au (5.90×10^{22} atoms/cm^3). At Au coverage below 0.5 ML for $SrTiO_3$ and 0.3 ML for S-TiO_2, 2D-islands growth is dominant. For HOPG support, however, large 3D-islands (large lateral size) are grown even at very small Au coverage. In the case of sputtered (Sp)-HOPG, we observed 3D-islands classified into two groups, small and large ones.

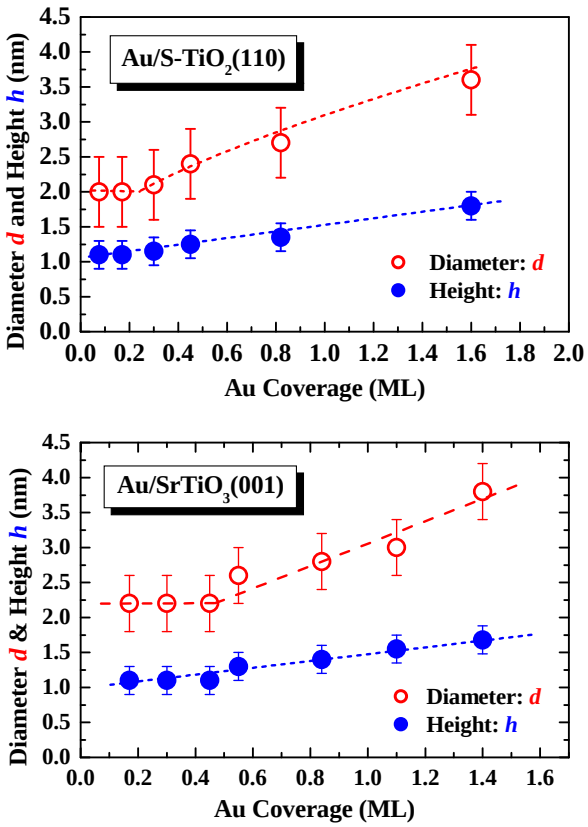

FIG. 3. Diameter *d* (open circles) and height *h* (full circles) of Au nano-particles grown on S-TiO_2(110) (upper) and on $SrTiO_3$(001) (lower) as a function of Au coverage, which are determined by MEIS.

Shown in Figs. 4(a) and (b) are the FE-SEM image taken for Au(0.7 ML)/Sp-HOPG at magnification of 600,000 and a part of that further magnified and contrast adjusted, respectively. Indeed, two groups; one distributed around ~0.5 nm and another around ~2 nm, are identified from Fig. 4(b) (see Fig. 4(c)). This is consistent with the MEIS analysis (see Fig. 6). The formation of such very small 3D-islands is ascribed to the fact that migration of Au atoms on the Sp-HOPG surface is suppressed because of the roughened surface and damage network acting as trap sites, which were induced by Ar^+ sputtering. The relatively large 3D-islands seem to grow around damaged sites neighboring relatively flat surface regions. Such a bimodal size distribution is intimately related to double peaks observed in Au 4f lines, as discussed later.

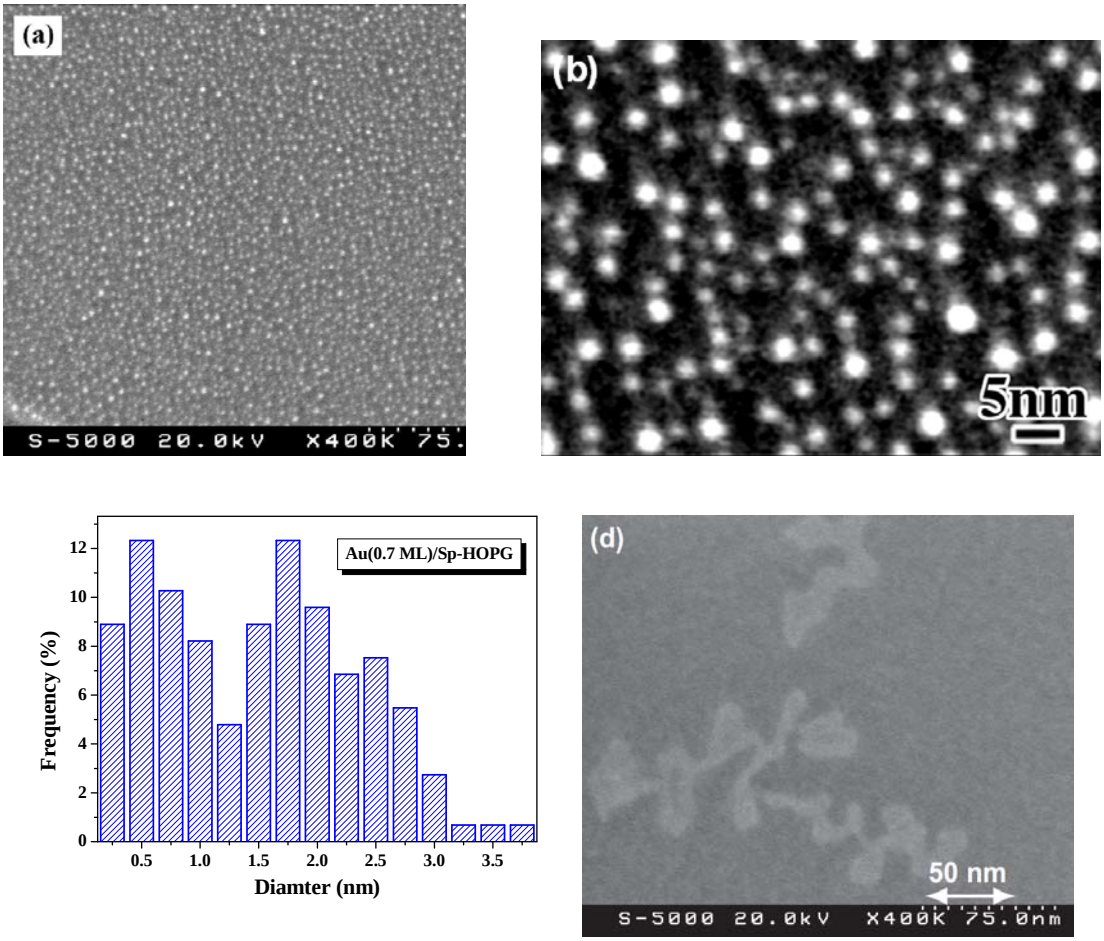

FIG. 4. (a) FE-SEM image taken for Au(0.7 ML)/Sp-HOPG and (b) the magnified one. (c) Particle-size distribution derived from the FE-SEM image. (d) FE-SEM image taken for Au(0.7 ML)/HOPG.

In contrast, Au deposition on HOPG leads to growth of split and tip branched islands, as shown in Fig. 4(d). The area of the island is considerably larger than that grown on Sp-HOPG at a same Au coverage. This was confirmed by MEIS analysis, although the shape and size were not determined exactly.

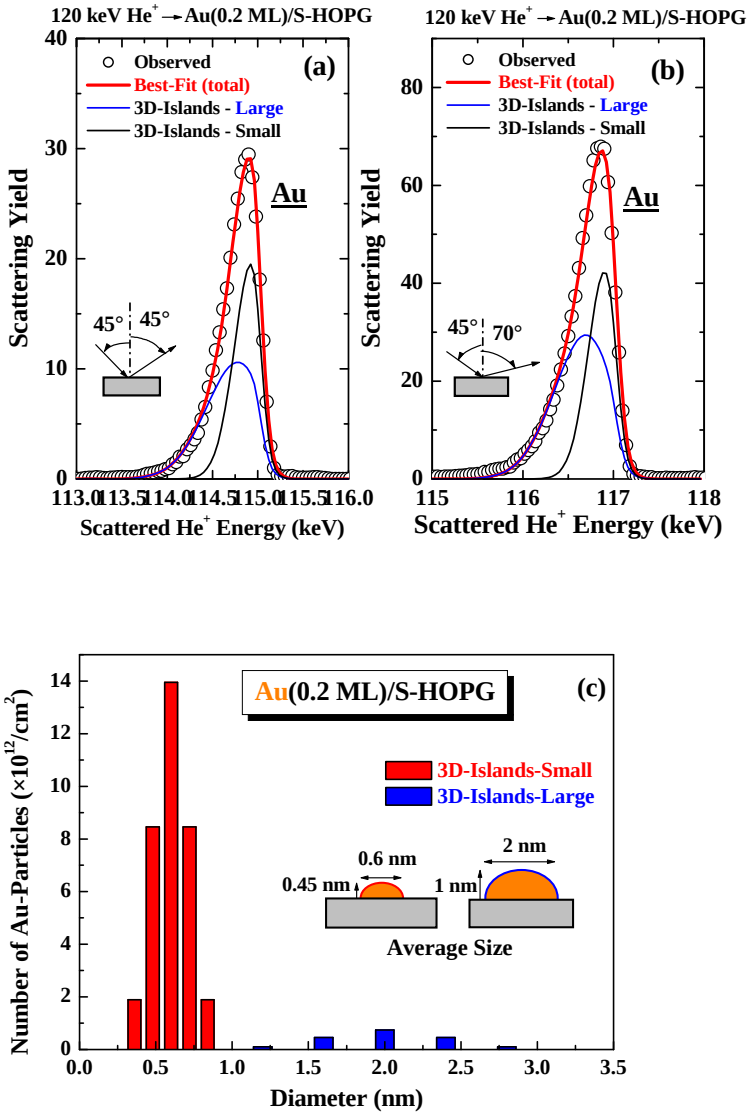

FIG. 5. MEIS spectra observed for 120 keV He^+ ions scattered from Au(0.2 ML)/Sp-HOPG (a) at incident and emerging angles of 45° and 45°, respectively and (b) at incident and emerging angles of 45° and 70°. The observed MEIS spectra are well reproduced assuming (c) bimodal size distribution, (i) average diameter of 0.6 nm and height of 0.46 nm and (ii) average diameter of 2.0 nm and height of 1.0 nm with standard deviation of 20 %. Thick red curves denote the best-fitted total spectra and thin black and blue curves indicate the components from (i) Au particles with smaller size and from (ii) those with larger size, respectively.

Figures 5 (a) and (b) show the MEIS spectra observed for Au(0.2 ML)/Sp-HOPG at different scattering conditions. Here, we assume a bimodal size distribution, (i) average diameter of 0.6 nm and height of 0.46 nm and (ii) average diameter of 2.0 nm and height of 1.0 nm[23]. The former cluster consists of 9~10 Au atoms and the latter ~124 Au atoms. The observed MEIS spectra are well reproduced assuming such two types of 3D-islands with a shape of partial sphere. The diameter and height are normally distributed with a fluctuation of 20 % (standard deviation), as indicated in Fig. 5(c). Note that there is another solution to get a best-fit spectrum instead of the assumption of the above small 3D-islands. That is to assume growth of an ultra-thin film whose thickness is fluctuated. In this case, the average thickness, fluctuation, and areal occupation ratio are fitting parameters. However, this assumption is inadequate, because the high-resolution FE-SEM observation indicates growth of small and large islands with an almost circular lateral shape whose sizes are fluctuated significantly.

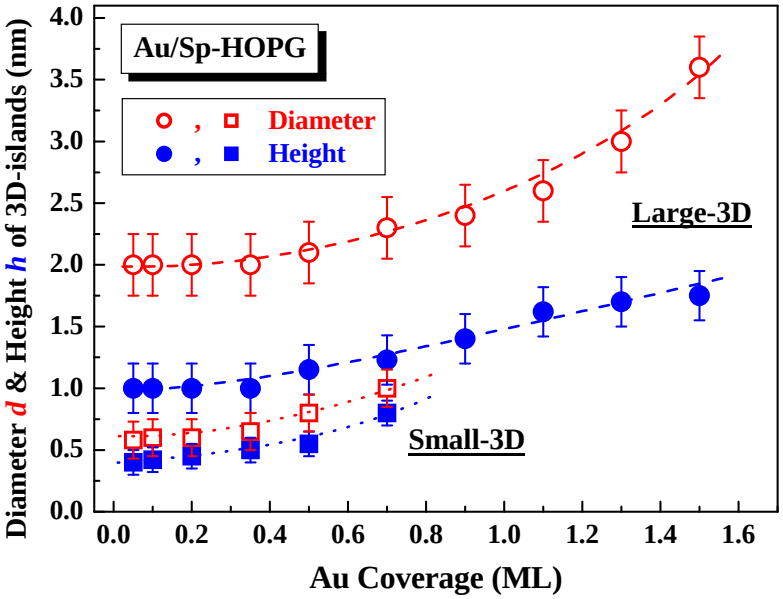

FIG. 6. Average diameter *d* (open symbols) and height *h* (closed symbols) for two types of 3D-islands as a function of Au coverage determined by MEIS. Circles denote large 3D-islands and squares small 3D-islands.

Figure 6 shows average diameter *d* and height *h* for two types of 3D-islands as a function of Au coverage determined by MEIS analysis. The areal occupation ratio of ~30 % for Au particles observed by FE-SEM (see Fig. 4(b)) is compatible with that of

25 % derived from MEIS analysis. Such a bimodal size distribution is also confirmed by correlation between the intensity of the Au $4f_{7/2}$ line and the surface areas of Au-particles derived from MEIS. Figure 7 shows the relative intensities of the two Au $4f_{7/2}$ components and the surface areas of small- and large-size Au particles as a function of Au coverage. Apparently, the Au $4f_{7/2}$ component with a higher E_B value is well correlated with smaller 3D-islands and that with lower E_B value is correlated with larger 3D-islands.

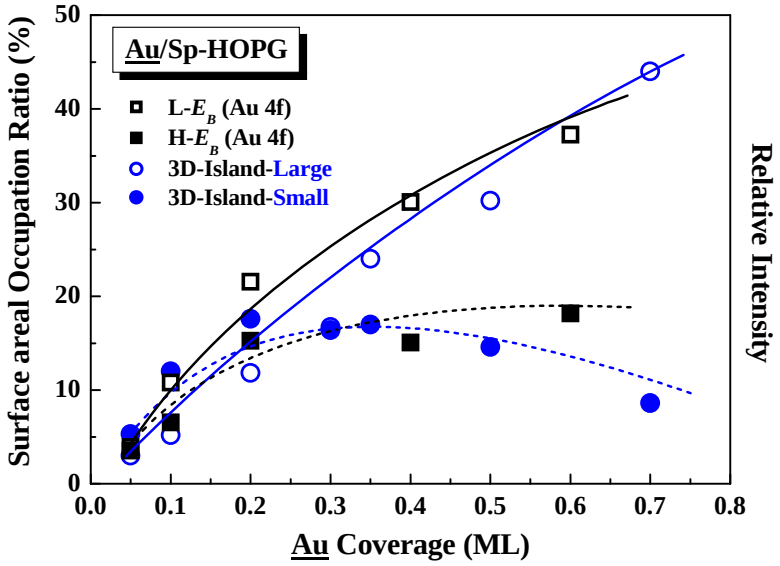

FIG. 7. Relative intensity of the two Au 4f lines with lower (open squares) and higher (full squares) E_B values and occupation ratios surface area for large (open circles) and small (full circles) 3D-islands, as a function of Au coverage.

As mentioned previously, we observed double peaks in Au $4f_{5/2,7/2}$ core level spectra for Sp-HOPG substrates. Figure 8 indicates the Au 4f spectra taken at photon energy of 140 eV under normal emission condition. Here, the spectra were best-fitted using the Voigt functions. The component with a higher E_B (H-E_B) becomes pronounced with decreasing Au coverage below 0.6 ML, while that with a lower E_B (L-E_B) dominates at higher Au coverage. The relative intensity of the (L-E_B) component increases almost proportionately to square root of Au coverage. This behavior is similar to that of the areal occupation ratio of the small 3D-islands determined by MEIS. On the other hand, the (H-E_B) component is well correlated with that of the small 3D-islands (not shown here). Shown in Fig. 9 are the E_B values of Au $4f_{7/2}$ for

Sp-HOPG and HOPG substrates as a function of Au coverage. Apparently, no E_B shift is seen for Au/HOPG, as shown previously (Fig. 2). In contrast, the E_B value of the (L-E_B) component approaches the E_B value of 84.0 eV at Au coverage above 0.4 ML corresponding to that of Au bulk. The E_B value of the (H-E_B) component decreases steeply with increasing Au coverage but does not reach the bulk E_B value. The (H-E_B) component is weakened with increasing Au coverage and not identified at Au coverage above 1.5 ML. Büttner and Oelhafen[19] first observed the two components in Au 4f spectra, one with considerably higher E_B shift and another with an E_B coinciding with the Au bulk component for Sp-HOPG and amorphous carbon supports but not for HOPG. They inferred a bimodal size distribution and the component with a higher E_B originating from extremely small Au particles. This is clearly evidenced by the present MEIS and FE-SEM observations, as described before.

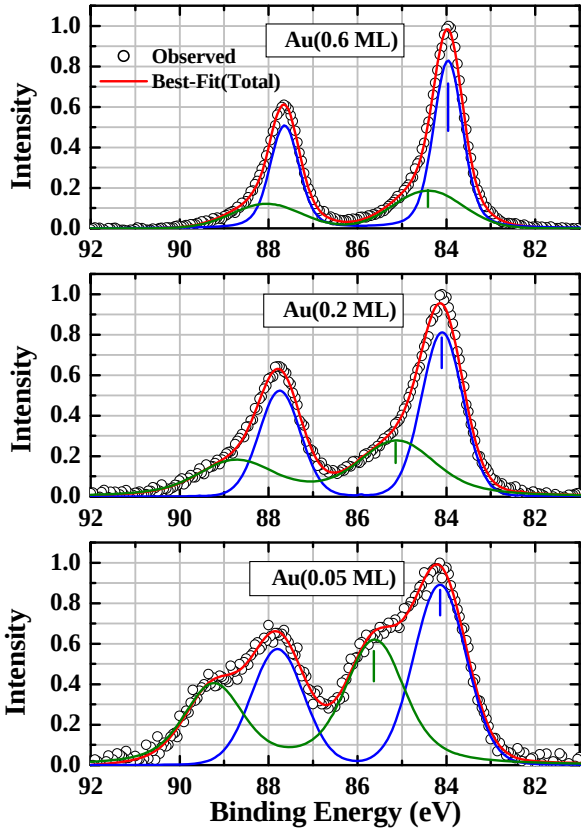

FIG. 8. Au 4f spectra taken for Au(0.05, 0.2, 0.6 ML)/Sp-HOPG at photon energy of 140 eV under normal emission condition. The observed spectra are decomposed into two components with higher (dotted) and lower (solid) E_B shifts.

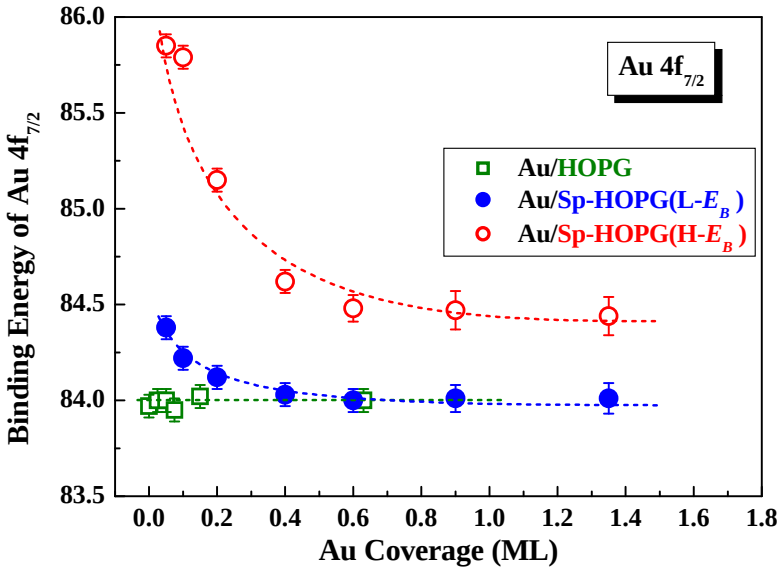

FIG. 9. Binding energy of Au $4f_{7/2}$ line observed for HOPG (squares) and Sp-HOPG (circles) substrates as a function of Au coverage. Components with higher and lower E_B values are indicated by open and closed circles, respectively.

From the results described above, it is clarified that the smaller the Au-particle size, the higher the E_B shift of Au 4f and the E_B shift is independent of substrate species. This assures one of the final state effect occurring for small Au nano-particles. Figure 10 indicates the E_B shift of Au $4f_{7/2}$ for various kinds of supports as a function of number of Au atoms per particle (n_A), which is determined by high-resolution MEIS analysis. Only the data for dominant 3D-growth are selected in this figure. Note that FE-SEM gives a lateral size but cannot identify 2D-islands, while MEIS is able to determine the height of 2D-islands but not the lateral size. It is clearly seen that the E_B shift depend on the number of Au atoms per particle not on support species. The E_B value increases exponentially with decreasing n_A below ~ 100 atoms, corresponding to V = ~1.7 nm^3. On the other hand, the E_B value gradually decreases with increasing n_A above ~ 100 atoms and approaches 0 at n_A = ~1,800 atoms ($d \cong$ 5 nm, if hemisphere is assumed) (not shown here). It is intriguing to point out that the Au particles with a number of Au atoms below 70 are non-metallic. Note that the number of 70 atoms per particle is widely recognized as a critical size (value) of metal nano-particles for a metal-nonmetal transition[5]. Such a situation is quite reasonable because a smaller number of valence electrons and the localized nature for nonmetal Au particles weaken

and delay the screening of a positive core hole created by photoemission. The average E_B shift $< \Delta E >_p$ is expressed approximately by

$$< \Delta E >_p = 1.63 \exp(-6.12\ \zeta) + 0.3 \qquad for\ \zeta < 1$$
$$= \frac{0.6\ \zeta}{\zeta^2 + 1} \qquad for\ \zeta > 1 \qquad (\zeta \equiv V / V_C) \tag{1}$$

This expression is useful for estimating the average size of Au particles from Au 4f E_B shift and vice versa.

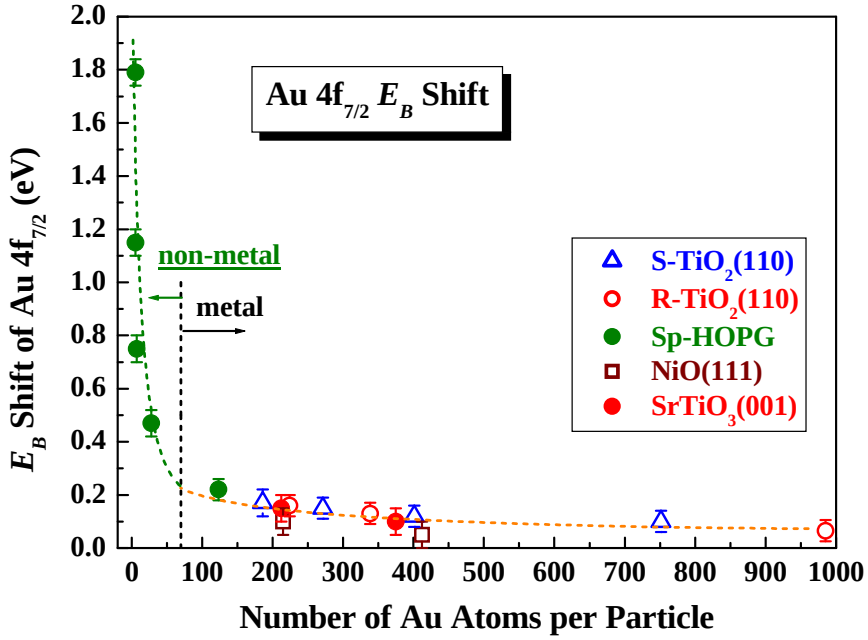

FIG. 10. E_B shift of Au $4f_{7/2}$ for R- and S-TiO_2(110), $SrTiO_3$(001), NiO(111) and Sp-HOPG supports as a function of number of Au atoms per particle determined by MEIS. Curves are drawn to guide the eyes. Dotted line indicates a critical number (70) of Au atoms per particle for metal-nonmetal transition.

Now, we consider the final state effect quantitatively based on a simple model. Hövel et al.[16] analyzed the E_B shift due to the final state effect assuming a sphere as a particle shape and a photo-hole left at center of the sphere. However, such an assumption seems nonrealistic, because the decay time of Au 4f state is roughly estimated to be several fs[30,31] and thus the Au 4f vacancy still survives when the photoelectron leaves surface of an Au-nano-particle. We assume that an Au 4f vacancy is created at a depth of an escape depth (λ) of photoelectrons as an average traveling length. In the present experimental condition, λ ranges from 0.3 to 0.5 nm[32].

The average energy shift $<\Delta E>$ is thus given by

$$< \Delta E > = < \Delta E >_{in} + \int_0^{\infty} \frac{\alpha\, e^2}{(\lambda + vt)^2} exp(-t/\tau)\; v\; dt$$
$$= < \Delta E >_{in} + \frac{\alpha\, e^2}{v\tau} \int_0^{\infty} \frac{exp(-\eta)}{(\beta + \eta)^2}\, d\eta, \qquad \beta \equiv \lambda/(v\tau) \tag{2}$$

where e is the electron charge, v the velocity of photoelectrons from the Au 4f state, and $< \Delta E >_{in}$ an energy loss of the photoelectron during traveling within an Au particle. The relaxation time τ to screen out the Au 4f vacancy is scaled from the time when the photoelectron just leaves the Au surface and the effective charge of the Au 4f vacancy is expressed by $+\alpha\, e$ (α < 1) at t = 0. Here, we must note that the E_B shift of Au $4f_{7/2}$ for Au nano-particles is measured relatively from the observed E_B value of 84.0 eV for Au bulk. Therefore, the E_B shift for an Au particle $< \Delta E >_p$ is expressed by

$$< \Delta E >_p = \frac{\alpha\, e^2\; exp(-\beta)}{v\tau} \int_0^{\infty} \frac{exp(-\eta)}{\eta^2}\, d\eta - \frac{\alpha\, e^2\; exp(-\beta_0)}{v\tau_0} \int_{\beta_0}^{\infty} \frac{exp(-\eta)}{\eta^2}\, d\eta, \tag{3}$$

where τ_0 is the relaxation time for bulk Au and $\beta_0 \equiv \lambda/(v\tau_0)$. The second term is negligibly small compared with the first term, because τ for small nano-particles should be much longer than τ_0. So, hereafter we neglect the second term. Based on the above model, we estimate roughly the screening coefficient α. For Au(0.6 ML)/S-TiO_2(110), we observed the E_B shift of +0.14±0.03 eV (±0.03 eV: peak resolution) and the Au-nano-particles are well approximated by partial spheres with average diameter of 2.7 nm and height of 1.4 nm (no 2D-islands). We adopt a value of 0.4 nm as an escape depth[32] for the Au $4f_{7/2}$ photoelectrons at ωA = 140 eV. The relation (α, τ) reproducing the observed E_B shift is indicated in Fig. 11. If a moving length of 0.5 - 1 nm of conduction electrons (Fermi velocity: v_F = 1.39×10^6 m/s) completes screening the Au 4f vacancy, corresponding relaxation time ranges from 0.36 to 0.72 fs. Then α takes a value of 0.053±0.003 estimated from Fig. 11. Note that $+\alpha\, e$ is the effective charge of the Au 4f vacancy at t = 0 (when leaving an Au-particle surface). Using this α value, the relaxation time for metallic Au nano-particles is estimated to be 2 fs at V = 3 nm^3 (n_A = 177) and 0.04 fs at V = 30 nm^3. If α is fixed for a photoelectron inside the metallic region, the relaxation time τ increase exponentially with decreasing V. This α value is considerably smaller than that (0.4

– 0.5) reported previously[13,16,18] based on the model proposed by Hövel et al.[16]. Indeed, for the extremely small Au particles (nonmetal) on Sp-HOPG, we must take a larger α value ranging from 0.14 up to 0.52 and the relaxation time becomes longer above several fs to reproduce the high E_B shifts. For such an extremely small nonmetal particles, screening is not completed until an electron is provided by the substrate to fill the Au 4f vacancy and it probably takes a time more than several fs. Unfortunately, it is difficult to determine experimentally the α and τ values independently, because they depend on the particle size. We also observed the peak shifts of Au 5d line (E_B: ~6 eV) for Au/Sp-HOPG (not shown here). In contrast to the Au 4f line, the Au 5d line takes a constant E_B value of 6.1 eV for Au coverage above ~0.6 ML and shifts toward lower E_B below ~0.4 ML (c.f. Fig. 2). The lower E_B shifts probably comes from band narrowing due to reduction of the atomic orbital-overlap[19,33]. This suggests a very short relaxation time less than 0.1 fs for the positive hole created in the valence band. Intuitively, a valence hole seems to be screened promptly by surrounding nearly-free electrons. On the other hand, the decay time of Au 4f is roughly estimated to be longer than 1 fs [30] and the screening of the Au 4f hole by outer-bound electrons seems not very efficient.

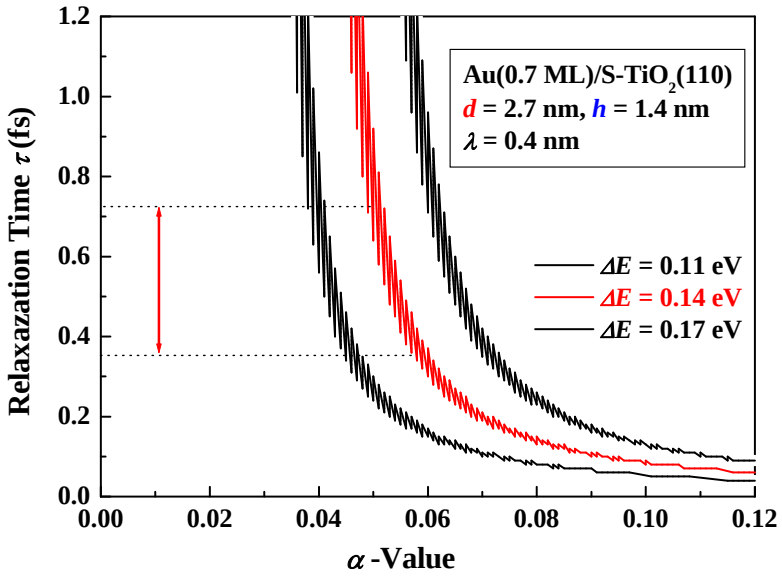

FIG. 11. (α, τ) relation satisfying the E_B shift of 0.14±0.03 eV, which was observed for Au(0.7 ML)/S-TiO_2(110). Black curves correspond to E_B shifts of 0.11 and 0.17 eV.

Finally, we consider the possibility to judge the electronic charge transfer at Au-particle/support interfaces (initial state) by Au 4f E_B shifts. Note that the electronic charge transfer discussed here corresponds to a hybridization of valence electrons at the Au/support interface resulting in a redistribution of electron density and does not mean positive or negative charging of each Au atom of an Au particle. As discussed above, the final state effect unambiguously emerges for Au nano-particles with a volume below ~30 nm^3 (n_A = 1,800), because the E_B shifts are well correlated with the number of Au atoms per particle and pronounced higher E_B shifts are seen for Au/Sp-HOPG although Au-C bonding is quite unlikely. For small Au particles consisting of Au atoms below ~ 100, a strong final state effect takes place and disturbs the detection of an initial E_B shift. For relatively large particles, the screening effect becomes pronounced and thus diminishes the electric filed of interface dipoles except for that of peripheral dipoles. There are some reports trying to separate the contributions to the core level shifts from the initial and final state effects by measuring characteristic X rays (E_{MN}) and Auger lines (E_{MNN})[34-36]. In spite of many efforts, some ambiguities arise from uncertainties of the energy levels in one- and two-hole states and of the states of valence electrons. This degrades the reliability of this method to evaluate the contributions from initial and final state effects separately. Therefore, it is difficult to detect the interface dipoles induced by hybridization of electronic states of valence electrons except for chemical bonding between Au and support giving a large E_B shift. However, local work functions and core level shifts of the elements of supports may give the information about the interface dipoles.

IV. CONCLUSION

The effect of a positive charge left to a small metal particle immediately after photoemission, so called the final state effect is studied quantitatively for Au 4f E_B shifts. The size and shape of Au-nano-particles are determined by high-resolution MEIS combined with FE-SEM. The shape of Au nano-particles is well approximated by a partial sphere with diameter d and height h except for HOPG support. It is found that the E_B shift is well expressed as a function of the number of Au atoms per particle (n_A), in other word the volume of Au nano-particle (if assume the atomic number density of Au nano-particles independent of particle size) and independent of support species. The E_B shift of Au $4f_{7/2}$ changes dramatically at a critical number of Au atoms of 70

corresponding to a critical volume of ~ 1 nm^3, where metal-nonmetal transition takes place. In the nonmetal region, the E_B shift increases steeply almost exponentially with decreasing n_A and in contrast, gradually decreases with increasing n_A in the metallic region. The effect of the positive charge of an Au 4f vacancy created by photoemission is expressed by the relaxation time τ and the effective charge $+\alpha e$ when the photoelectron just leaves the Au particle surface ($\alpha < 1$). The screening coefficient α takes a value around 0.05 for metallic Au particles and ranges from 0.15 to 0.5 for nonmetal particles (n_A < 70). The higher E_B shift is enhanced remarkably by a delayed screening effect of valence electrons due to a smaller number of valence electrons and the localized character of nonmetal particles which results in a long relaxation time. In contrast to the Au 4f line, no significant E_B shift was observed for Au $5d_{3/2}$ line (E_B: ~6 eV) for Au coverage above 0.6 ML. This suggests a very short relaxation time less than 0.1 fs for the positive hole created in the valence band.

ACKNOWLEDGMENTS

The authors would like to thank Prof. H. Namba for maintaining the PES system at BL-8. Special thanks are also due to Dr. M. Kohyama for useful discussion and comments. This work was supported partly by Japan Science and Technology Agency, JST, CREST.

References

[1] M. Haruta, T. Kobayashi, H. Sano, and N. Yamada, Chem. Lett. **2**, 405 (1987).

[2] M. Haruta, Catal. Today **36** (1997) 153.

[3] M. Valden, X. Lai, and D.W. Goodman, Science **281** (1998) 1647.

[4] G.K. Wertheim, S.B. DiCenzo, D.N.E. Buchanan, Phys. Rev. **B 33**, 5384 (1986).

[5] H-J. Freund, Surf. Sci. **500** (2002) 271.

[6] Y. Maeda, M. Okumura, S. Tsubota, M. Kohyama, and M. Haruta, Appl. Surf. Sci. **222** (2004) 409.

[7] A. Sanchez, S. Abbet, U. Heiz, W.D. Schneider, H. Häkkinen, R.N. Barnett, and U. Landman, J. Phys. Chem. **A 103** (1999) 9573.

[8] L.M. Molina and B. Hammer, Phys. Rev. **B 69** (2004) 155424.

[9] K. Okazaki, Y. Morikawa, S. Tanaka, K. Tanaka, and M. Kohyama, Phys. Rev. **B 69** (2004) 235404.

[10] T. Minato, T. Susaki, S. Shiraki, H.S. Kato, M. Kawai, and K.-I. Aika, Surf. Sci. **566-568**, (2004). 1012.

[11] J.G. Wang and B. Hammer, Phys. Rev. Lett. **97** (2006) 136107.

[12] T. Okazawa, M. Kohyama, and Y. Kido, Surf. Sci. **600** (2006) 4430.

[13] A. Howard, D.N.S. Clark, C.E.J. Mitchell, R.G. Egdell, and V.R. Dhanak, Surf. Sci. **518** (2002) 210.

[14] M.S. Chen and D.W. Goodman, Catal. Today **111** (2006) 22.

[15] G.K. Wertheim, S.B. DiCenzo, and S.E. Youngquist, Phys. Rev. Lett. **51** (1983) 2310.

[16] H. Hövel, B. Grimm, M. Pollmann, and B. Reihl, Phys. Rev. Lett. **81** (1998) 4608.

[17] T. Ohgi and D. Fujita, Phys. Rev. **B 66** (2002) 115410.

[18] A. Tanaka, Y. Takeda, T. Nagasawa, and K. Takahashi, Solid State Com. **126** (2003) 191.

[19] M. Büttner and P. Oelhafen, Surf. Sci. **600** (2006) 1170.

[20] Y. Kido, H. Namba, T. Nishimura, A. Ikeda, Y. Yan, and A. Yagishita, Nucl. Instrum. Methods **B 136-138**, 798 (1998).

[21] H. Namba, M. Obara, D. Kawakami, T. Nishimura, Y. Yan, A. Yagishita, and Y. Kido, J. Synchrotron Rad. **5** (1998) 557.

[22] T. Nishimura, A. Ikeda, and Y. Kido, Rev. Sci. Instrum. **69** (1998) 1671.

[23] A. Iwamoto, T. Okazawa, T. Akita, I. Vickridge, and Y. Kido, Nucl. Instrum. Methods **B266** (2008) 965.

[24] T. Nishimura, A. Ikeda, H. Namba, T. Morishita, and Y. Kido, Surf. Sci. **421** (1999) 273.

[25] T. Okazawa, M. Fujiwara, T. Nishimura, T. Akita, M. Kohyama, and Y. Kido, Surf. Sci. **600** (2006) 1331.

[26] T. Okazawa , T. Nishizawa, T. Nishimura, and Y. Kido, Phys. Rev. **B 75** (2007) 033413.

[27] T. Nishimura, Y. Hoshino, T. Okazawa, and Y.Kido, Phys. Rev. **B 77** (2008) 073405.

[28] B. Blum, R.C. Salvarezza, and A.J. Ariva, J. Vac. Sci. Technol. **B 17** (1999) 2431.

[29] J. Lindhard and M. Scharff, K. Dan. Vidensk. Selsk. Mat.-Fys. Medd. **27** (15) (1953).

[30] B. Crasemann, M.H. Chen, and H. Mark, J. Opt. Soc. Am. **B 1** (1984) 224.

[31] M. Drescher, M. Hentschel, R. Kienberger, M. Uiberacker, V. Yakovlev, A. Schrinzi, Th. Westerwalbesloh, U. Kleineberg, U. Heinzmann, and F. Krausz, Nature **419** (2002) 803.

[32] S. Tanuma, T. Shiratori, T. Kimura, K. Goto, S. Ichimura, and C.J. Powell, Surf. Interface Anal. **37** (2005) 833.

[33] S.B. DoCenzo, S.D. Berry, and E.H. Hartford, Jr., Phys. Rev. **B 38** (1989) 8465.

[34] G.G. Kleiman, R. Landers, P.A. Nascente, and S.G.C. de Castero, Phys. Rev. **B 46** (1992) 4405.

[35] K. Luo, X. Lai, C.-W Yi, K.A. Davies, K.K. Gath, and D.W. Goodman, J. Phys. Chem. **109**, (2005) 4064.

[36] I. Lopez-Salido, D.C. Lim, R. Dietsche, N. Bertram, and Y.D. Kim, J. Phys. Chem. **B 110** (2006) 1128.